First principles nonequilibrium plasma mixing

C. Ticknor,[1] S. D. Herring,[1] F. Lambert,[2] L. A. Collins,[1] and J. D. Kress[1]
[1]*Los Alamos National Laboratory, Los Alamos, New Mexico 87545, USA*
[2]*CEA, DAM, DIF, F-91297 Arpajon, France*
(Received 30 July 2013; published 27 January 2014)

We have performed nonequilibrium classical and quantum-mechanical molecular dynamics simulations that follow the interpenetration of deuterium-tritium (DT) and carbon (C) components through an interface initially in hydrostatic and thermal equilibrium. We concentrate on the warm, dense matter regime with initial densities of 2.5–5.5 g/cm^3 and temperatures from 10 to 100 eV. The classical treatment employs a Yukawa pair-potential with the parameters adjusted to the plasma conditions, and the quantum treatment rests on an orbital-free density functional theory at the Thomas-Fermi-Dirac level. For times greater than about a picosecond, the component concentrations evolve in accordance with Fick's law for a classically diffusing fluid with the motion, though, described by the mutual diffusion coefficient of the mixed system rather than the self-diffusion of the individual components. For shorter times, microscopic processes control the clearly non-Fickian dynamics and require a detailed representation of the electron probability density in space and time.

DOI: 10.1103/PhysRevE.89.013108 PACS number(s): 52.27.Gr, 52.65.Yy

I. INTRODUCTION

Interfaces between interpenetrating fluids represent a common physical environment encountered in a diverse set of circumstances, including zone boundaries in gas and ice giant planets [1], the ablator-fuel divide in inertial confinement fusion (ICF) capsules [2–6], the creation of complex chemical mixtures [7–9], and the initiation region for self-assembly of nanostructures [10,11]. While some of these examples must function at a microscopic level, such as in the case of self-assembly or chemical mixtures, others would appear to operate on a macroscopic scale of general hydrodynamics, such as planetary layers and ICF capsule implosions. Yet, at a fundamental level, all interface dynamics involve microscopic processes. Therefore, for large-scale systems, a crucial question becomes on what spatial and temporal timescales does the transition from a microscopic to macroscopic representation occur? This question has ramifications in the realm of materials at extreme conditions. To investigate the interface dynamics in this regime, we concentrate on a representative problem given by the initial interfacial mixing at the ablator-fuel boundary of an imploding ICF capsule.

A particularly crucial stage occurs at the peak velocity of the ablator impact on the fuel in which small imperfections at the interface can grow into hydrodynamical instabilities, such as Rayleigh-Taylor [6], that have deleterious effects on the implosion process. This situation occurs for compressed materials (∼5–20 g/cm^3) at intermediate temperatures (10–50 eV), the traditional warm, dense matter regime (WDM) consisting of a soup of atoms, ions, and electrons that usually requires a quantal treatment. Such microscopic properties as electron thermal conductivities, viscosity, and diffusion play significant roles in controlling the magnitude of the instabilities and mixing [12]. The diffusion also determines the distance over which contaminants such as the ablator material can penetrate and degrade the fuel [4,5]. These properties, however, are generally determined from equilibrium simulations although the interface exists in a decidedly nonequilibrium state. Our investigation focuses on the diffusion process through the first large-scale molecular dynamics (MD) simulations of a plastic-fuel (C-DT) interface using an orbital-free finite-temperature density functional theory (OF-DFT) approach that treats the electrons quantum mechanically through a Thomas-Fermi-Dirac approximation. In addition, we also employed a classical MD method with a screened pair potential to gauge quantum-mechanical and sample-size effects. We examine the interface evolution in general and specifically the approach to a classical hydrodynamical (Fickian) behavior and the microscopic processes governing the diffusive interpenetration.

II. FORMULATION

To address this complex, nonequilibrium system, we perform both classical and quantum molecular dynamics numerical simulations of an ideal C/DT interface and directly observe the atomistic mixing. For the quantal case, we invoke the Born-Oppenheimer approximation and separate the electronic and nuclear motions. The N_i nuclei move according to classical equations of motion (EOM) in response to a force on the ion from the interactions with other ions and a quantal contribution from the N_e electrons at a fixed ion configuration within an isokinetic ensemble [13]. The force due to the electrons derives from a finite-temperature orbital-free density functional theory [14] treatment in a Thomas-Fermi-Dirac mode with the kinetic-entropic form of Perrot [15], the electron-ion interaction from a regularization prescription, and the exchange-correlation from a local density Perdew-Zunger form [16]. The technique has proven highly effective in spanning the WDM regime, producing equilibrium mass transport quantities and equations-of-state for both single and multicomponent dense plasmas [17–21] that agree well with the computationally more intense Kohn-Sham DFT at low temperatures and with simpler models such as the one-component plasma at high temperatures [14].

We also performed classical molecular dynamics simulations using the scalable parallel short-range molecular dynamics (SPaSM) code [22] for a Yukawa pair-potential, $V_{ij}(R_{ij}) = \frac{Z_i Z_j e^2}{R_{ij}} e^{-R_{ij}/\lambda}$, where $Z_i e$ is the effective charge of atom i, λ is the screening length, and R_{ij} is the distance

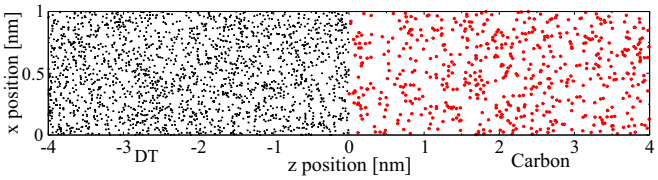

FIG. 1. (Color online) A schematic diagram of the initial condition: DT (small black dots) and C (large red circles) start on either side of $z = 0$ at $t = 0$ in hydrostatic and thermal equilibrium.

between atoms i and j. The regularization prescription from the OF-DFT also determines the effective charge $Z_i e$ for each species, and a linearized Thomas-Fermi theory [23] prescription sets the screening length λ. This choice of effective charge and screening length assumes a uniform plasma for a given species, either DT or C. The ions evolve temporally according to the classical EOM with a force determined from the spatial derivative of the potential V_{ij} for a microcanonical ensemble, which maintained within about a percent of the initial temperature.

For both the classical and quantum MD simulations, we consider a long box of length L_z and cross section L_x by L_y divided at $z = 0$ with $N_{\rm DT}$ hydrogenic atoms in the left-hand compartment and $N_{\rm C}$ carbon atoms in the right, shown schematically in Fig. 1. We impose periodic boundary conditions in all three directions, which in turn gives rise to two interfaces at $z = 0$ and $z = \pm L_z/2$. A single surrogate particle of atomic weight 2.5 g/mol serves for DT. Holding the temperature fixed at T, each side is independently equilibrated by varying the number of particles until the total pressures become equal [$P_{\rm DT} = P_{\rm C}$]. This prescription establishes an initial condition of hydrostatic equilibrium at the same temperature. We then allow the two components to mix.

For the orbital-free molecular dynamics (OFMD) case, we find that the requisite C density needed to enforce hydrostatic equilibrium with a DT sample at 2.5 g/cm^3 remains at about 5.4 g/cm^3 over the temperature range of 10 to 100 eV. We use a volume of approximately $0.6 \times 0.6 \times 10$ nm^3 having 1200 DT and 556 C atoms. The long dimension sets a limit on the maximum duration with the simulations terminating once particles from either interface meet in the middle. We also ran simulations for a volume of $1.4 \times 1.4 \times 16$ nm^3 with over 10^4 particles, which yielded results agreeing within a few percent with those of the standard volume. Typical time steps ranged between 0.025 and 0.008 fs for temperatures between 10 and 100 eV, respectively.

Despite the difference in the treatment of the particle interactions, the Yukawa required about the same initial C density to obtain hydrostatic equilibrium, 5.5 g/cm^3. Between 10 and 100 eV, the effective charge for hydrogen $Z_{\rm H}$ changes from 0.72 to 0.93 while that for carbon, $Z_{\rm C}$ ranges from 2.6 to 4.1. For a given temperature and density, the screening parameters λ for DT and C are about the same and vary from 0.9 to $1.9a_{\rm B}$ over the temperature range. Neither parameter changes during a given simulation.

Additionally, we employed the Yukawa simulations to test convergence in volume and particle number. Since properties of the interpenetrating species come from cross-sectional averages, we first examined the sensitivity for a cell length, fixed at the OFMD case ($L_z = 16$ nm), to an area varied between 1×1 and 18×18 nm^2 and total particle numbers from about 10^4 to 3×10^6 ions. A number of ions of around 10^4 proved sufficient to reach convergence in the properties and physical structure of the evolving sample. With a set cross-sectional area, we varied the length of the cell to support simulations of up to 3 ps duration. The area, particle number, and cell length studies with Yukawa potentials served to validate the basic OFMD findings, which were more restricted in sample size and temporal range.

We performed equilibrium calculations in order to determine basic static and transport properties for comparison with the nonequilibrium interface simulations. We consider a fixed number of atoms $N = N_{\rm DT} + N_{\rm C}$ and volume that yielded the average of the densities of the initial two sides. At a given temperature, equilibrium MD simulations with both OFMD and Yukawa produced trajectories of positions and velocities of the ions from which self ($D^e_{\rm DT}$,$D^e_{\rm C}$) and mutual (D^e_{12}) diffusion coefficients were extracted [20]. We designate the equilibrium results by a superscript e. Typically, samples of 500 atoms and trajectories of at least 10^4 time steps proved sufficient to calculate converged equilibrium properties to within a few percent. For the mutual diffusion coefficient, we employ a value of unity for the thermodynamic factor Q, consistent with calculations based on an analysis [24] of the pair-correlation functions from the equilibrium simulations.

III. RESULTS AND DISCUSSION

The conditions described by Fig. 1 as delineated in the discussion above indicate a system initially in hydrostatic and thermal equilibrium with a density difference of only a factor of two and would seem to presage a rather prosaic interpenetration. Such a view though would prove erroneous as an examination of the plasma coupling coefficient Γ [25] would indicate. This parameter gives a qualitative measure of the state of a partially ionized medium, ranging from domination by interactions (strongly coupled: $\Gamma \gg 1$) to domination by kinetics (weakly coupled: $\Gamma \ll 1$). For our initial conditions at 10 eV, $\Gamma_{\rm C} \approx 10$ and $\Gamma_{\rm DT} \approx 1$. The temperature mainly controls these values with the valence shells of both C and hydrogen nearly completely ionized. For the fully mixed result, $\Gamma_{\rm mix} \approx 3$. On the other hand, at 100 eV, $\Gamma_{\rm C} \approx 2.1$, $\Gamma_{\rm DT} \approx 0.2$, and $\Gamma_{\rm mix} \approx 0.6$. Thus, the components cover a broad range of plasma conditions from fully segregated to fully mixed and dramatically change both temporally and spatially as the system evolves.

In Fig. 2, we present a representative case of the nonequilibrium OFMD simulations for a temperature of 40 eV, showing the cross-sectionally-averaged number densities $n_i(z,t)$ of the DT (circles) and C (squares) ions at various times. The two components display comparable interpenetration. Many macroscopic prescriptions exist for characterizing the width of the interface [8,9]; the simplest arises from the application of Fick's diffusion law, [$dn_i/dt = D_i^f \nabla^2 n_i$], starting from $n_i(z,0)$ a step function. An analytical solution of the form

$$n_i(z,t) = \frac{A_i}{2}\mathrm{erfc}\left(\frac{z - z_0^i}{2w_i(t)}\right), \qquad (1)$$

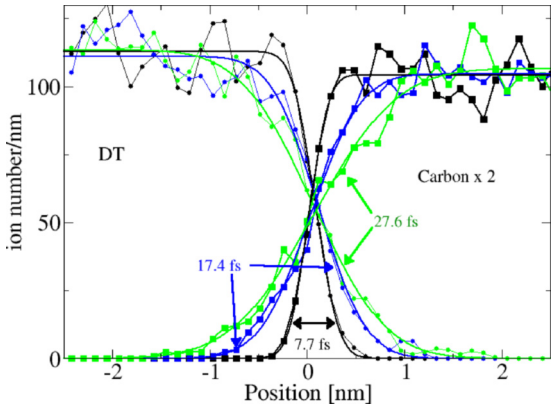

FIG. 2. (Color online) The OFMD simulated line density and fits are shown for the DT-C interface for 40 eV at times 7.7 (black), 17.4 (blue, gray), and 27.6 (green, light gray) fs. Both the line densities of DT (circles) and C (squares) are shown. The error function fits are shown as solid lines. The time of each curve is also labeled with an arrow.

yields the temporal evolution, where A_i is the amplitude, z_0^i is the location of the interface, and w_i is the width of the interface such that $w_i(t) = \sqrt{D_i^f t}$, with D_i^f a diffusion coefficient. The degree to which the simulations of the number density as a function of z and time for the individual species follows this form gives a measure of the departure of the microscopic evolution from a purely macroscopic diffusion picture. To this end, we performed a nonlinear least-squares fit of the cross-sectionally integrated number density $n_i(z,t)$ to the error-function expression in Eq. (1) and designate with a superscript f the resulting diffusion coefficient. The results roughly follow the simple fits; however, some deviations manifest themselves in the leading edges and in density depletions near the interface as seen at later times. An important test of the pressure matching procedure is to track z_0^i, the position of the interface. The fitted values of z_0^i start at zero and move only a small amount over the duration of any simulation, typically less than 1% of L_z.

Figure 3 displays the Yukawa (a) and OFMD (b) widths, extracted from the error function fits as a function of time for temperatures of 10 and 60 eV for DT (symbols). We focus first on the behavior of the Yukawa widths in Fig. 3(a). The greater range of the Yukawa simulations in sample size and trajectory length permit more accurate quantitative analysis, which in turn can help illuminate the OFMD results. At late times ($t > 100$ fs), the widths approach a purely diffusive behavior, achieving the characteristic $t^{\frac{1}{2}}$ form. From this asymptotic behavior, we can therefore directly extract a diffusion coefficient D_i^f and plot the resulting expression $w_i(t) = \sqrt{D_i^f t}$ as solid lines in Fig. 3. On the other hand, the departure from the pure Fickian behavior at early times emphasizes the importance of microscopic processes. To account more realistically for the overall time behavior, we employ an alternative fit for the width:

$$w_i(t) = \sqrt{D_i^f t}(1 - e^{-\sqrt{t/\tau}}). \qquad (2)$$

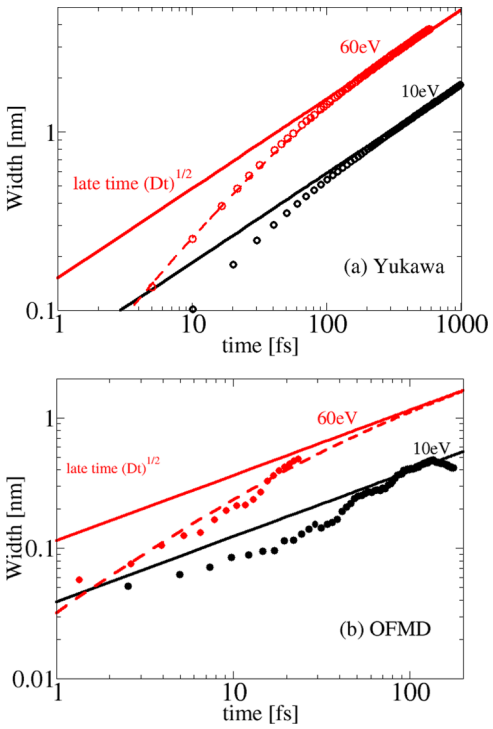

FIG. 3. (Color online) Comparison of extracted widths as a function of time for (a) Yukawa and (b) OFMD simulations. Widths from the asymptotic fit $\sqrt{D_{\rm DT}^f t}$ (solid lines); the function from Eq. (2) is shown as dashed line for 60 eV; and widths from error-function fits (symbols). The temperatures are 10 eV for lower black curves and 60 eV for upper red curves.

At early times, the width is a linear function of time, which corresponds to ballistic behavior with the two components experiencing only small numbers of collisions and moving almost as if free particles. As time passes, the particles experience more interactions, and the conditions around the interface become more complicated. The parameter τ provides an approximate measure for the transition from the ballistic to the intermediate state. Eventually, at long times, the mixing becomes substantial and Fickian behavior ensues with the transition coming at approximately 20τ. For the Yukawa simulations, we find that the two-parameter fit of Eq. (2) works well over the entire range as indicted by the example at 60 eV (dashed line) and that τ remains roughly constant over the temperature range ($\tau \approx 17$ fs). The diffusion coefficients agree to within a fraction of a percent with those derived from a fit to the purely asymptotic form (solid line).

We next examine the temporal evolution of the OFMD widths in Fig. 3(b). Due to the shorter trajectories necessitated by the large computer resources required, only the 10-eV simulation reached purely Fickian asymptotic behavior. By performing the Yukawa fits over the same limited trajectory range as the OFMD, we find that a fit to only the asymptotic form ($t^{\frac{1}{2}}$) generally underestimates the diffusion coefficient. To determine an upper bound, we fit the OFMD width at 10 eV to Eq. (2) and extract $\tau \approx 9$ fs. Assuming the same temperature independence of τ as discovered in the Yukawa case and fitting the restricted OFMD trajectories to Eq. (2)

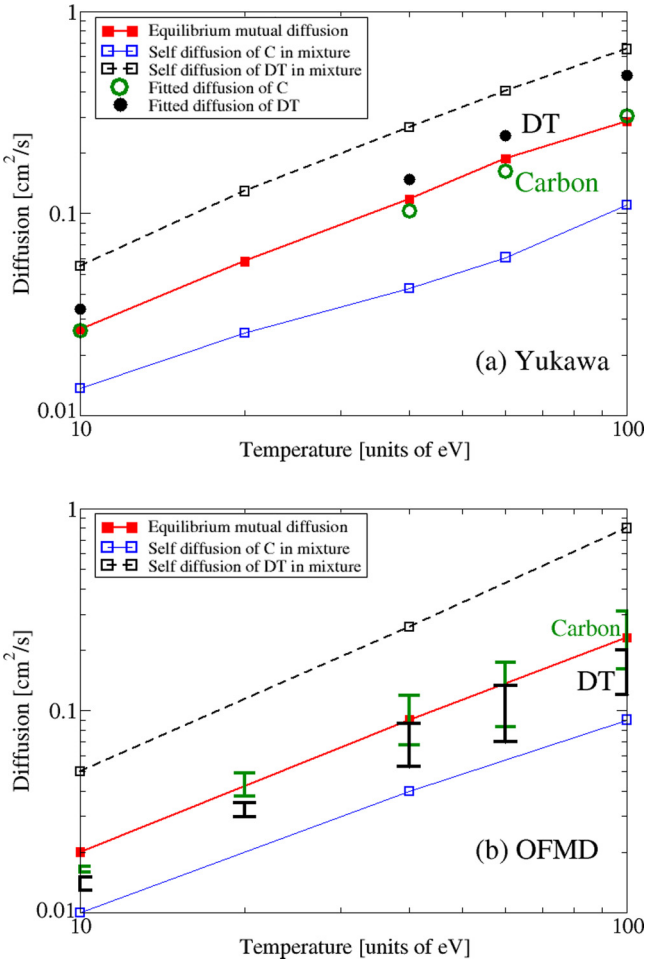

FIG. 4. (Color online) Diffusion coefficients (a) Yukawa and (b) OFMD simulations: the fitted widths from the nonequilibrium simulations for DT are shown as black symbols and C as green (light gray) symbols. Also shown are the equilibrium diffusion coefficients. The self-diffusion for DT are open black squares with dashed lines and for C are open blue squares with a solid line. The mutual diffusion is shown as solid line with red squares (middle curve).

with τ fixed determines another value for diffusion coefficient. The two values then give a lower and upper bound to the OFMD diffusion coefficients at the higher temperatures. This analysis indicates that the OFMD, compared to the Yukawa, reaches Fickian behavior at a considerably shorter time and has a smaller effective diffusion coefficient by almost a factor of two. This latter observation we now explore in more detail.

We first concentrate on the effective diffusion coefficients from the Yukawa simulations in Fig. 4(a). As indicated above, reasonable values of the Fickian diffusion coefficients can be determined from the asymptotic temporal trends. We plot the diffusion coefficients extracted at late times from the error-function fits for DT (black dots) and C (green circles) for Yukawa interface simulations and compare to equilibrium calculations of self and mutual diffusion coefficients. Interestingly, the DT and C diffuse at about equal rates across the interface, which at first seems counterintuitive, given that at a specific temperature, the more massive component should trail its lighter counterpart. The behavior of the equilibrium self-diffusion coefficients D^e_α seems to confirm this contention. However, the interface poses a more complex situation in that the particle densities differ by a factor of two and that the dynamics occur within a highly nonequilibrium state. Despite these complications, both DT and C appear to diffuse (intermix) according to the equilibrium mutual diffusion coefficient (D^e_{12}) with a possible small departure at the higher temperatures. We emphasize that this finding emerges exclusively from the full microscopic simulations of the interface.

We now turn to the OFMD simulations in Fig. 4(b) in which we present the fitted diffusion coefficients for DT (black symbols) and C (green symbols), as well as the self and mutual diffusion coefficients for the DT and C mixture from equilibrium calculations. The OFMD results mirror those for the Yukawa with the DT and C diffusing across the interface at about the same rate as given roughly by the equilibrium mutual diffusion coefficient. As observed from the analysis of the widths, the associated diffusion rates for the OFMD remain about half those for the Yukawa. This difference may arise from many factors, but certainly the explicit representation of the electrons in the OFMD must play a role. As opposed to the Yukawa parameters for each species that are fixed to the initial conditions, the quantum mechanics (electron density) physically adjusts the "effective charges and screening lengths" locally (at the ion scale) and temporally in response to the large gradients in the Coulomb fields (ion densities of DT and C) as the interpenetration evolves away from the interface.

Finally, in many applications, the distance $d_i(t)$ to which a specific component penetrates into another within a given time can provide important information on its ability to affect other processes with the mixed system. A simple estimate of the diffusion distance is $2\sqrt{Dt}$ with the appropriate diffusion coefficient D, in this case D_{12}. For example, at 10 eV, the DT would travel about 30 Å into the carbon in about 1 ps. We emphasize though that this rule only applies once the system has reach the hydrodynamical (Fickian) limit.

IV. CONCLUSION

Within the warm, dense matter regime, we have performed nonequilibrium classical and quantum mechanical molecular dynamics simulations in order to follow the interpenetration of deuterium-tritium and carbon components through an interface. For times greater than about a picosecond, the two concentrations evolve in accordance with Fick's law for a classically diffusing fluid though with the motion best described by the mutual diffusion coefficient of the mixed system rather than the self-diffusion of the individual components. For shorter times, microscopic processes control the clearly non-Fickian dynamics at the interface. We have demonstrated that even this seemingly simple case of an interface at hydrostatic [$P_{\rm DT} = P_{\rm C}$] and thermal [$T_{\rm DT} = T_{\rm C}$] equilibrium with only a concentration gradient exhibits complex behavior that evolves through several stages with time. The MD methods have considerable versatility and can handle more complicated conditions such as pressure gradients and external fields.

ACKNOWLEDGMENTS

The authors gratefully acknowledge support from the Advanced Simulation and Computing Program (ASC), science campaigns 1 and 4, computing resources under ASC's CCC, and LANL, which is operated by LANS, LLC for the NNSA of the U.S. DOE under Contract No. DE-AC52-06NA25396. This work was performed under the auspices of an agreement between CEA/DAM and NNSA/DP on cooperation on fundamental science.

[1] R. Redmer, T. R. Mattson, N. Nettleman, and M. French, Icarus **211**, 798 (2011); J. J. Fortney, M. S. Marley, and J. W. Barnes, Astrophys. J. **659**, 1661 (2007); R. Helled, J. D. Anderson, M. Podolak, and G. Schubert, *ibid.* **726**, 15 (2011).

[2] S. H. Glenzer *et al.*, Science **327**, 1228 (2010); C. K. Li *et al.*, *ibid.* **327**, 1231 (2010).

[3] D. Clery, Science **327**, 514 (2010); **334**, 449 (2011).

[4] J. R. Rygg, J. A. Frenje, C. K. Li, F. H. Séguin, R. D. Petrasso, V. Yu. Glebov, D. D. Meyerhofer, T. C. Sangster, and C. Stoeckl, Phys. Rev. Lett. **98**, 215002 (2007).

[5] D. C. Wilson *et al.*, Phys. Plasmas **18**, 112707 (2011).

[6] B. A. Hammel *et al.*, High Energy Density Phys. **6**, 171 (2010).

[7] L. B. Partay, G. Horvat, and P. Jedlovsky, Phys. Chem. Chem. Phys. **10**, 4754 (2008); J. B. Buhn, P. A. Bopp, and M. J. Hampe, J. Mol. Liqs. **125**, 187 (2006).

[8] D. Beysens and M. Robert, J. Chem. Phys. **87**, 3056 (1987).

[9] S. Senapati and M. L. Berkowitz, Phys. Rev. Lett. **87**, 176101 (2001).

[10] D. L. Cheung and S. A. F. Bon, Phys. Rev. Lett. **102**, 066103 (2009); A. Varghese and S. Datta, Phys. Rev. E **85**, 056104 (2012).

[11] Y. Adda, J. Philibert, and V. Pontikis, Phys. Rev. B **85**, 144121 (2012).

[12] F. Lambert and V. Recoules, Phys. Rev. E **86**, 026405 (2012).

[13] P. Minary, G. J. Martyna, and M. E. Tuckerman, J. Chem. Phys. **118**, 2510 (2003).

[14] F. Lambert, J. Clerouin, and G. Zerah, Phys. Rev. E **73**, 016403 (2006).

[15] F. Perrot, Phys. Rev. A **20**, 586 (1979).

[16] J. P. Perdew and A. Zunger, Phys. Rev. B **23**, 5048 (1981).

[17] J. D. Kress, J. S. Cohen, D. P. Kilcrease, D. A. Horner, and L. A. Collins, Phys. Rev. E **83**, 026404 (2011).

[18] J.D. Kress, J. S. Cohen, D. A. Horner, F. Lambert, and L. A. Collins, Phys. Rev. E **82**, 036404 (2010).

[19] D. A. Horner, J. D. Kress, and L. A. Collins, Phys. Rev. B **77**, 064102 (2008).

[20] D. A. Horner, F. Lambert, J. D. Kress, and L. A. Collins, Phys. Rev. B **80**, 024305 (2009).

[21] J. F. Daniel, L. Kazandjian, and G. Zerah, Phys. Plasmas **19**, 122712 (2012).

[22] P. S. Lomdahl, P. Tamayo, N. Gronbech-Jensen, and D. M. Beazley, *Proceedings of the Supercomputing Conference* (IEEE Computer Society Press, Losa Alamitos, CA, United States, 1993), p. 520.

[23] D. Gilles, F. Lambert, J. Clerouin, and G. Salin, High Energy Density Phys. **3**, 95 (2007).

[24] M. Schoen and C. Hoheisel, Molec. Phys. **52**, 33 (1984).

[25] The plasma coupling coefficient Γ for a single species is given by $\frac{Z^2e^2}{a_i k_B T}$, with Z, the effective charge; T, the temperature; and $a_i = (\frac{3}{4\pi n_i})^{\frac{1}{3}}$, the ion-sphere radius for a number density of n_i.